The Astrophysical Journal Letters, 820:L29 (7pp), 2016 April 1 doi:10.3847/2041-8205/820/2/L29

MICROWAVE IMAGING OF A HOT FLUX ROPE STRUCTURE DURING THE PRE-IMPULSIVE STAGE OF AN ERUPTIVE M7.7 SOLAR FLARE

Zhao Wu[1], Yao Chen[1], Guangli Huang[2], Hiroshi Nakajima[3], Hongqiang Song[1], Victor Melnikov[4], Wei Liu[5], Gang Li[6], Kalugodu Chandrashekhar[1], and Fangran Jiao[1]
[1] Shandong Provincial Key Laboratory of Optical Astronomy and Solar-Terrestrial Environment, and Institute of Space Sciences, Shandong University, Weihai, Shandong 264209, China; yaochen@sdu.edu.cn
[2] Purple Mountain Observatory, Chinese Academy of Sciences (CAS), Nanjing, 210008, China
[3] Nobeyama Radio Observatory, NAOJ, 462-2 Nobeyama, Minamimaki, Minamisaku, Nagano 384-1305, Japan
[4] Central Astronomical Observatory at Pulkovo, Russian Academy of Sciences, Saint Petersburg 196140, Russia
[5] W. W. Hansen Experimental Physics Laboratory, Stanford University, Stanford, CA 94305, USA
[6] Department of Space Science and CSPAR, University of Alabama in Huntsville, Huntsville, AL 35899, USA
Received 2015 December 9; accepted 2016 March 8; published 2016 March 24

ABSTRACT

Corona structures and processes during the pre-impulsive stage of solar eruption are crucial to understanding the physics leading to the subsequent explosive energy release. Here we present the first microwave imaging study of a hot flux rope structure during the pre-impulsive stage of an eruptive M7.7 solar flare, with the Nobeyama Radioheliograph at 17 GHz. The flux rope is also observed by the *SDO*/AIA in its hot passbands of 94 and 131 Å. In the microwave data, it is revealed as an overall arcade-like structure consisting of several intensity enhancements bridged by generally weak emissions, with brightness temperatures (T_B) varying from ~10,000 K to ~20,000 K. Locations of microwave intensity enhancements along the structure remain relatively fixed at certain specific parts of the flux rope, indicating that the distribution of emitting electrons is affected by the large-scale magnetic configuration of the twisted flux rope. Wavelet analysis shows a pronounced 2 minute period of the microwave T_B variation during the pre-impulsive stage of interest. The period agrees well with that reported for AIA sunward-contracting loops and upward ejective plasmoids (suggested to be reconnection outflows). This suggests that both periodicities are controlled by the same reconnection process that takes place intermittently at a 2 minute timescale. We infer that at least a part of the emission is excited by non-thermal energetic electrons via the gyro-synchrotron mechanism. The study demonstrates the potential of microwave imaging in exploring the flux rope magnetic geometry and relevant reconnection process during the onset of solar eruption.

Key words: magnetic reconnection – Sun: corona – Sun: flares – Sun: radio radiation

Supporting material: animation

1. INTRODUCTION

Coronal flux ropes, i.e., magnetic structures consisting of field lines twisted around each other, are believed to be one of the major pre-eruptive agents of solar coronal mass ejections (CMEs) with free magnetic energy to drive the eruption (e.g., Low & Hundhausen 1995; Chen 1996; Forbes 2000; Low 2001). Their existence has been revealed by latest observational studies using high-quality imaging data of the Atmospheric Imaging Assembly (AIA; Lemen et al. 2012) on board the *Solar Dynamics Observatory* (*SDO*; Pesnell et al. 2012) via its high-temperature passbands at 131 Å (~11 MK) and 94 Å (~7 MK) (Zhang et al. 2012; Cheng et al. 2013; Song et al. 2014, 2015; Sun et al. 2014). It has been therefore suggested that such a pre-eruption flux rope contains plasmas as hot as ~10 MK, possibly heated by an underlying reconnection process. Yet, it remains elusive about how the reconnection works to heat or even form the flux rope and whether non-thermal energetic electrons are produced during the process.

An eruptive M7.7 flare took place on 2012 July 19, with valuable observations that may contribute to resolve the above issue. The event was well-observed by the *SDO* and *Reuven Ramaty High Energy Solar Spectroscopic Imager* (*RHESSI*; Lin et al. 2002) spacecraft, as well as the ground-based microwave Nobeyama Radioheliograph (NoRH; Nakajima et al. 1994; Takano et al. 1997). A number of studies on the event have been published, revealing many intriguing evolutionary details of the flare (e.g., Liu 2013; Liu et al. 2013; Patsourakos et al. 2013; Krucker & Battaglia 2014; Morgachev et al. 2014; Sun et al. 2014). It was established that the eruption was associated with a pre-existing high-temperature flux rope structure according to AIA/*SDO*. The flux rope was likely formed by a preceding C4.5 flare that took place ~7 hr earlier. The rope stayed and evolved in the corona for several hours before its eventual eruption leading to the M7.7 flare and a fast CME propagating at a speed $>1000\,\mathrm{km\,s^{-1}}$ (Patsourakos et al. 2013).

Liu et al. (2013) presented a comprehensive study on the event using both *SDO* and *RHESSI* data. They found that the event belongs to the well-known Masuda-type flare with a hard X-ray (HXR) source high lying in the corona above the flaring soft X-ray (SXR) arcade (Masuda et al. 1994). They examined the spacing difference between X-ray sources at various energy bands, as well as the temperature distribution with a forward-modeling differential emission measure (DEM) analysis (Aschwanden et al. 2013), to infer sites of plasma heating and electron acceleration induced by reconnection. Along with other detailed measurements on contracting/shrinking plasma loops and ejective plasmoids, they concluded that the primary loci of heating and electron acceleration were in the reconnection outflow regions, rather than the reconnection site itself. In addition, they also found that the reconnection outflows, as revealed by fast contracting loops and upward-

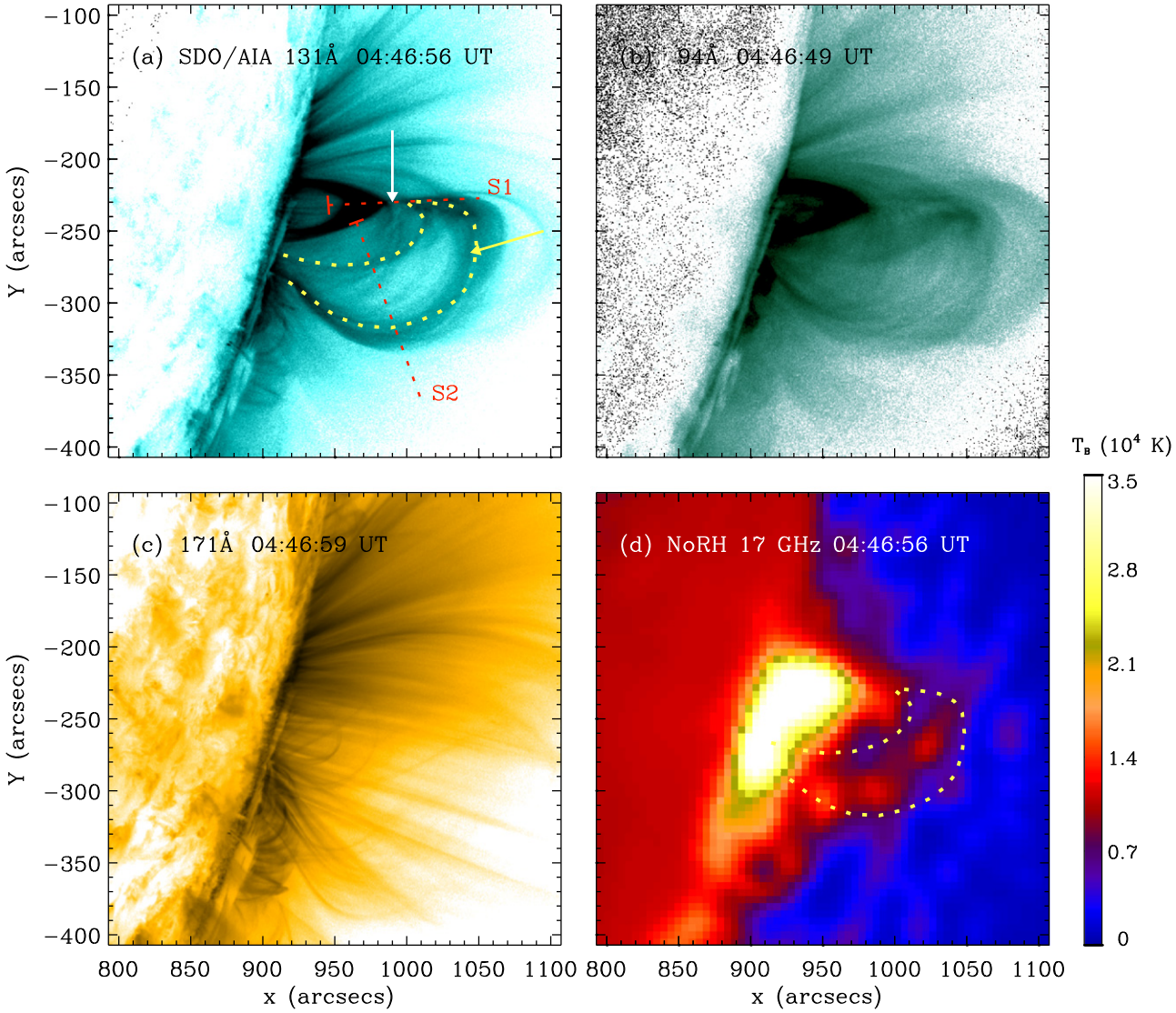

Figure 1. AIA and NoRH images at ~04:56 of the pre-impulsive phase of the M7.7 flare on 2012 July 19. Panels (a)–(c) present images in passbands of 131, 94, and 171 Å, and panel (d) presents the image of NoRH at 17 GHz. The yellow dashed curves in panel (a) delineate the flux rope structures in 131 Å that have been superposed onto the microwave image in panel (d). The white arrow in panel (a) points to the vertical thin current sheet structure. Slices S1 and S2 are used to plot the height-time maps shown in Figure 2. The short bars at the inner end of S1 and S2 indicate the starting point of the distance measurement along the slice.

(An animation of this figure is available.)

flowing plasmoids during the flare pre-impulsive stage, exhibited a quasi-periodic occurrence rate at ~2 minutes. This last finding is of close relevance to the study presented here.

Most previous studies of this event focused on the *SDO* and *RHESSI* data, while the microwave data of the event recorded by NoRH at 17 and 34 GHz have not been paid enough attention. The coronal microwave emission is contributed to by both thermal bremsstrahlung and non-thermal gyro-synchrotron mechanisms (e.g., Dulk 1985). Emission given by the latter carries valuable information about energetic electrons and magnetic field strength and geometry. Liu (2013) and Morgachev et al. (2014) analyzed the NoRH microwave data to reveal the spatial and velocity distributions of energetic electrons along loops of the major M7.7 flare, yet mainly during the impulsive stage. Here, we analyze the microwave data during the pre-impulsive stage focusing on the relatively weak, yet significant, microwave emission in the region corresponding to the hot AIA flux rope structure. To our knowledge, this is the first imaging study of a hot flux rope in the microwave regime. The study reveals valuable information about the flux rope structure and the generally weak reconnection process during the flare pre-impulsive stage. These are representative of major physical ingredients leading to the eventual solar eruption. Section 2 introduces more relevant details of the event, as already presented by other authors. The third section shows our major results on the microwave emission associated with the flux rope. The fourth section discusses the nature of coronal microwave emission, which is followed by the section of conclusions and discussion.

2. DATA ANALYSIS AND OVERVIEW OF THE M7.7 ERUPTIVE FLARE

The M7.7 flare occurred at 04:17 UT and peaked at 05:58 UT on 2012 July 19. It was a limb event from NOAA

AR 11520. The event can be separated into pre-impulsive (04:17 UT to 05:16 UT) and impulsive (05:16 UT to 05:43 UT) stages, according to the derivative of the *GOES* SXR light curves and the HXR 25–50 keV profiles (cf. Liu et al. 2013). The emission from the northern flare loop foot was partly occulted by the solar disk, allowing the above-the-loop-top source of the HXR emission to be observed. In Figures 1(a)–(c), we present the 131, 94, and 171 Å images observed at ~04:47 UT, during the pre-impulsive stage to show the pre-existing flux rope structure. The rope is best seen at 131 Å and is almost invisible at 171 Å, indicating it contains high-temperature plasmas. An accompanying animation of Figure 1 is available showing the evolution of the event. The yellow dashed curves in Figure 1(a) delineate the inferred outer border of the flux rope structure, within which some twisted structures can be clearly seen. In the 131 Å image, there exists a thin vertical structure connecting the tip of the cusp-like flare loops and the northern end of the flux rope (pointed by the white arrow), which has been recognized as the high-temperature current sheet along which reconnections took place (Liu et al. 2013).

In the pre-impulsive stage, the flux rope structure exhibited a slow-rising motion (see the animation of Figure 1). Reconnection outflows in the form of downward contracting arcades and ejective plasmoids have been observed along the current sheet structure (Liu 2013; Liu et al. 2013). Of particular interest is the quasi-periodic occurrence of these reconnection-induced features. Liu et al. (2013) found that there were 29 downward contracting arcades and 25 ejective plasmoids from 04:15 to 05:25 UT, i.e., the pre-impulsive phase (see their Figure 7). We repeated this analysis and show our result in Figure 2(a) with height-time maps along slice S1 (see Figure 1(a)). The red and black dashed tracks represent the upward- and downward-moving structures, respectively. We found 24 contracting arcades from 04:20 to 05:15 UT and 14 eruptive plasmoids from 04:20 and 04:50 UT, yielding an average occurrence rate of 2.3 and 2.1 minutes. Both outflows have their origin from the vertical current sheet structure that is indicated by the central long-dashed line in Figure 2(a). The linear-fitting speeds of these tracks are in a range of 10–60 km s^{-1} for the downward-moving structures and 50–400 km s^{-1} for the upward-moving structures. These results are consistent with those obtained by Liu et al. (2013), indicating the intermittent nature of the pre-impulsive reconnection. Here, we will examine whether this intermittency has imprints on the microwave emission that is likely related to energetic electrons. Note that, according to *RHESSI*, the coronal HXR emission within the flux rope at this stage is too weak to provide statistically meaningful photon counts.

For this purpose, we use the NoRH data recorded during the pre-impulsive stage of this event at both 17 and 34 GHz, with a 1 s cadence and beam size being ~17 arcsec for 17 GHz (shown in Figure 3(a)) and 8.7 arcsec for 34 GHz. According to the NoRH analysis manual (http://solar.nro.nao.ac.jp/norh/doc/; manual version 3.3), there are three different NoRH synthesis methods, named as Hanaoka, Koshix, and Fujiki programs, with the Koshix one being the most appropriate for analyzing diffuse sources such as the one studied here. So we mainly use this program for our study. For comparison, we also tried the Hanaoka program and found our main results are not affected.

In the pre-impulsive phase of the M7.7 flare, the activities of the Sun were limited to AR 11520 (there was no other bright

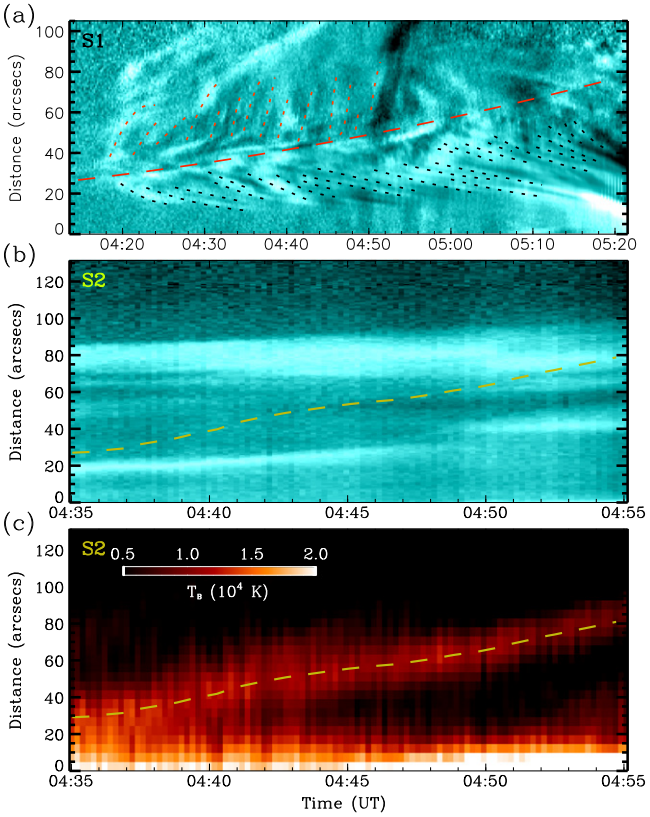

Figure 2. Height-time maps along slices S1 and S2. See Figure 1 for slice locations. Panel (a) is for AIA 131 Å to show the reconnection outflows, observed from 04:14 UT to 05:22 UT. Downward-contracting loops are indicated by black dashed lines, upward-moving plasmoids by red dashed lines. The middle red long-dashed line shows the reconnecting current sheet region. Panels (b) and (c) are height-time maps along S2 for AIA 131 Å and the brightness temperature data of NoRH at 17 GHz, respectively, from 04:35 UT to 04:55 UT. The NoRH data are synthesis images processed by the Koshix program with 12 s integration of the raw data. Dashed lines in panels (b) and (c) indicate the rising motion of the microwave structure.

active region), and the maximum brightness temperature (T_B) was roughly 30,000 K. Therefore, the noise in the NoRH raw images (before applying the CLEAN procedure) of the radio Sun is essentially determined by the system noise, which is given by the sum of the antenna temperature due to the quiet Sun and the receiver noise temperature. According to Takano et al. (1997), the system noise temperature for 1 s data is ~1000–1500 K for 17 GHz and ~6000 K for 34 GHz. In the synthesis of 17 GHz images, we set the CLEAN level to be 3000 K that is the default value and integrated 12 frames (12 s) of NoRH raw images before applying the CLEAN algorithm to further reduce the system noise. For 34 GHz data, we used the Hanaoka program (note the Koshix program is not applicable for the 34 GHz data) and found that in the flux rope region of interest T_B is considerably less than the corresponding sensitivity level (~6000 K). Therefore, in the following, we only analyze the 17 GHz data of NoRH.

3. MICROWAVE IMAGING OF THE PRE-IMPULSIVE HOT FLUX ROPE STRUCTURE

Coronal microwave sources were present around and above the cusp region following the earlier C4.5 flare, with enhanced activities during the pre-impulsive stage of the M7.7 flare. In Figure 1(d), we have overplotted the flux rope regime depicted

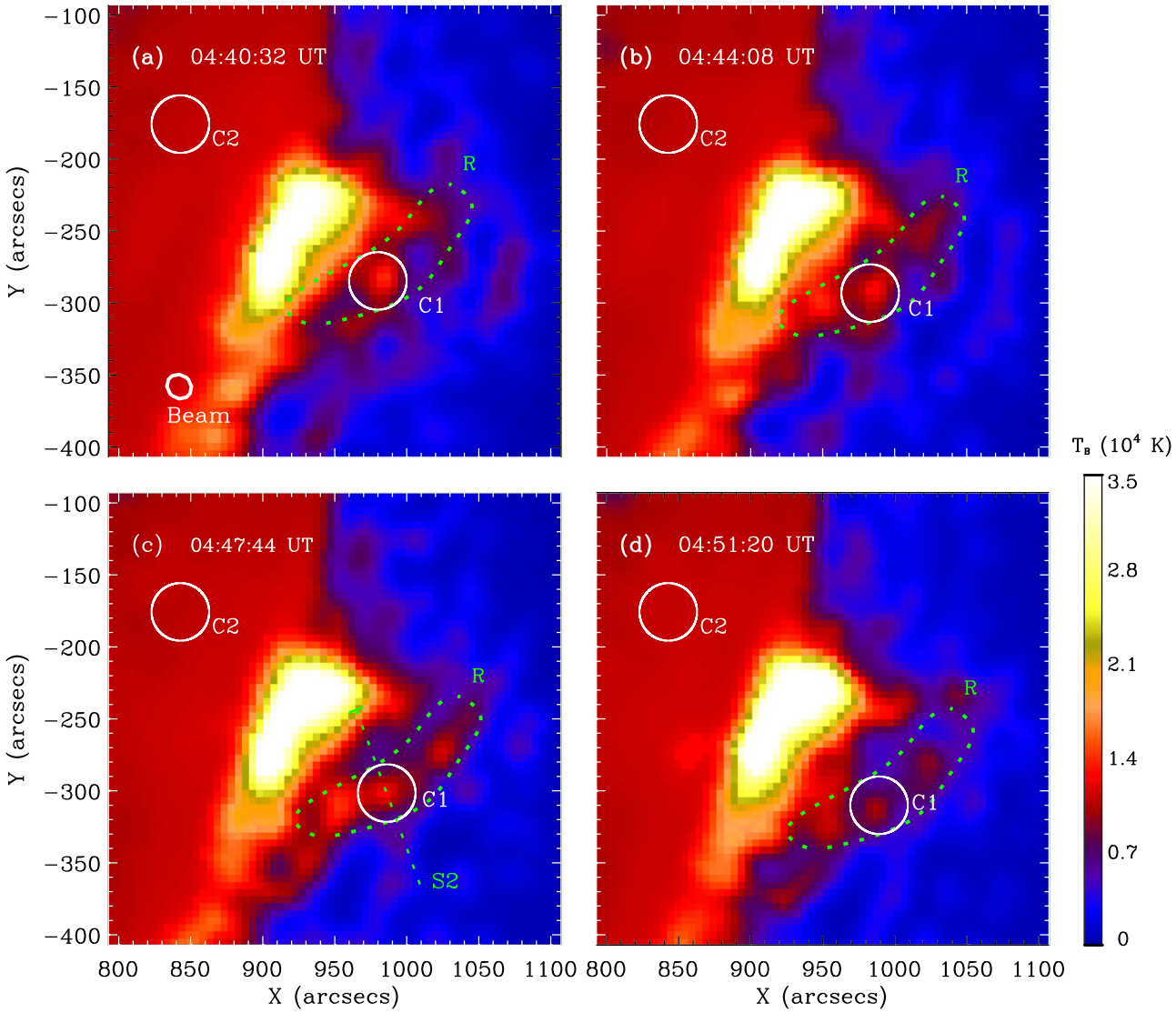

Figure 3. Image sequence of the NoRH 17 GHz microwave data from 04:40 UT to 04:52 UT, showing the brightness temperature (T_B). Region R indicates the overall microwave flux rope regime observed at 17 GHz, and circle C1 (C2) denotes the region surrounding the middle microwave intensity enhancement (the solar background) with radius ~20 arcsec. Both region R and circle C1 move outward along S2 with a projection speed of ~28 km s^{-1}. The beam size of NoRH 17 GHz is shown in panel (a). The accompanying animation has been presented with Figure 1.

by the dashed curves in Figure 1(a). It can be seen that some distinct yet relatively weak microwave sources appear in the middle part of the flux rope region. In Figure 3, we further present four snapshots of the NoRH microwave images. See also the animation accompanying Figure 1 for the evolutionary process from 04:35 UT to 04:55 UT. As mentioned, several similar bright structures (referred to as microwave islands) with $T_B \sim 10,000$ to over 20,000 K are present within the AIA 131 Å flux rope structure. Between adjacent sources, relatively weaker emission ($T_B \sim$ 10,000–14,000 K) exists. This forms an overall arcade-like microwave structure threaded by the localized brightness maxima. The number of these T_B maxima varies from three to five. Their T_B changes rapidly over time, yet their locations seem to be relatively fixed to specific parts of the large structure.

The arcade-like microwave structure is clearly separated from the bright flaring loop source, as seen from the second, third, and forth columns of Figure 3 and the animation of Figure 1. The overall microwave structure presents a gradually rising motion. This agrees with the very similar motion of the AIA flux rope structure, as shown by the height-time maps along slice S2 (see Figure 2(b) (for AIA 131 Å data) and Figure 2(c) (for NoRH 17 GHz data) from which we see that the trajectory of the microwave source (indicated by a long-dashed line) lies in the middle part of the flux rope structure. The average rising speed of microwave structure is ~28 km s^{-1}. This further supports the idea that the microwave arcade-like structure corresponds to the internal part of the hot flux rope observed in the AIA 131, 94 Å passbands. Note that it is not possible to tell which specific AIA structure in Figure 1 contains the microwave-emitting energetic electrons since both background and foreground structures are projected together onto the plane of the sky.

The energetic (or thermal) electrons accounting for the microwave emission are likely produced and filled into the flux rope by the ongoing reconnection during the pre-impulsive stage. The reconnection is revealed by the AIA-observed contracting arcades and upward ejection of plasmoids from the

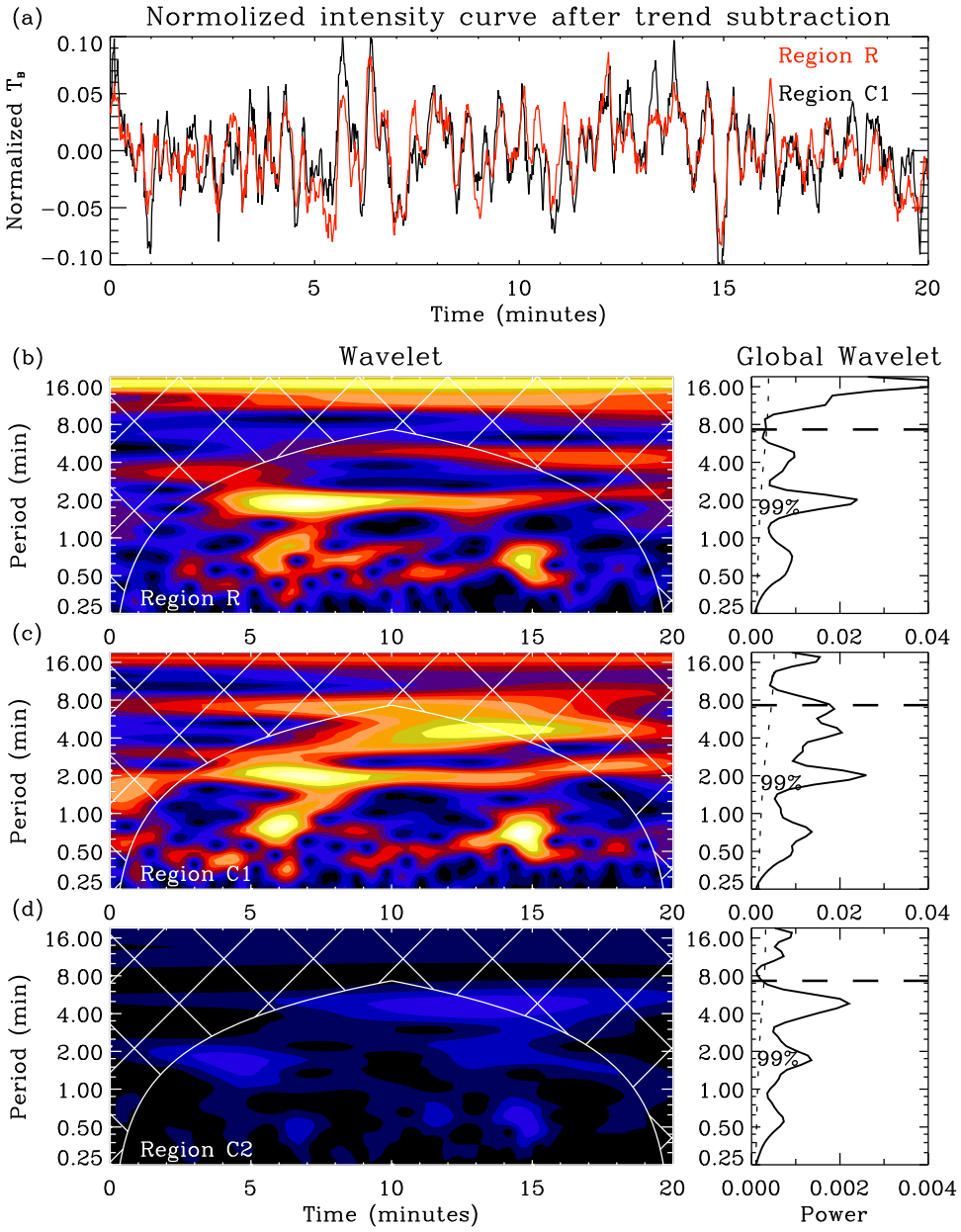

Figure 4. Wavelet analysis of the NoRH 17 GHz T_B temporal variations. Panel (a) shows the averaged T_B (normalized after trend subtraction) in region R and C2 from 04:35 UT to 04:55 UT. Panels (b) and (c) show the corresponding power spectra and the global power spectra given by wavelet analysis, respectively. Panel (d) is the wavelet results obtained for the data averaged (also normalized with trend subtraction) in C2 (see Figure 3) from 04:35 UT to 04:55 UT. The trend profile is obtained by taking average of the original T_B data every 400 s. Subtracting the long-term average trend does not affect the wavelet analysis result as long as the term is much longer than 2 minutes. The horizontal dashed lines in the global spectra indicate the significance level of 99%. Cross-hatched regions on the spectra show the cone of influence. Note that around 0.5–1 minutes there exists some spectral power. However, the corresponding spectral features last only for a few minutes with much less power than the 2 minute one, and the associated period varies in a relatively large range from 0.5 to 1 minutes. We therefore suggest that these periodicities are not significant.

current sheet structure, according to previous studies (e.g., Liu 2013; Liu et al. 2013). In order to find whether the intermittency associated with AIA reconnection outflows (see Figure 2) have some imprint on the microwave emission, we conduct wavelet analyses on the temporal profiles of T_B in the flux rope region.

To analyze the temporal variation of the microwave intensity, we first average the T_B values in region R for the overall flux rope region (defined in Figure 3), from 04:35 UT to 04:55 UT. The normalized T_B averages after subtracting the general variation trend are presented as the red plot in Figure 4 (a) and the obtained wavelet and global power spectra are shown in Figure 4(b), from which we see a significant period of 2 minutes that carries the strongest spectral power. Almost the same 2 minute period appears in a similar wavelet analysis for the normalized average T_B values in circle C1, which is selected to be centered around the middle microwave island and moving outward along S2.

For comparison, we also conduct wavelet analysis with the data representative of the quite-Sun microwave background in circle C2. See Figure 4(d) for the results. The power is much weaker, and no significant periodicity exists. This indicates that the above 2 minute periodicity is physical and indeed associated with the microwave flux rope structure.

Thus, we conclude that the microwave emission exhibits a significant 2 minute quasi-periodic oscillation. The period agrees well with that reported for the AIA sunward-contracting loops and upward ejective plasmoids (suggested to be reconnection outflows) during the same period (see Figure 2; Liu et al. 2013), indicating both quasi-periodicities have the same physical origins given by the pre-impulsive reconnection along the thin vertical current sheet.

4. DISCUSSION ON THE NATURE OF THE CORONAL MICROWAVE EMISSION

The first issue we should clarify is about the physical significance of the weak coronal microwave sources, i.e., whether the signals are real or produced artificially by the NoRH image synthesis procedure. As mentioned in Section 2, the NoRH system noise of 1 s data is ~1000–1500 K, and we have integrated 12 s of NoRH raw images before applying the CLEAN algorithm to further reduce the noise. With a CLEAN level set to be 3000 K, we suggest that sources observed at 17 GHz with $T_B > 3000$ K are real. The physical significance of these microwave sources are also supported by their location and dynamics that are highly correlated with the AIA structure.

Then, we need to infer whether the microwave sources are given by non-thermal energetic electrons via the gyro-synchrotron emission or by thermal electrons through the bremsstrahlung emission or by a combination of both (Dulk 1985). This is in general difficult since we cannot take direct measurements on thermal and magnetic parameters of the corona sources. One traditional way to resolve this issue is to examine the rough microwave spectrum using the NoRH two-frequency data (e.g., Narukage et al. 2014); however, as mentioned, the 34 GHz data are below the NoRH sensitivity and not usable here. Nevertheless, there still exists a qualitative approach to infer the nature of the microwave emission.

It is well known that the plasma temperature and emission measure can be deduced with the DEM method. Given these parameters, the thermal bremsstrahlung contribution can be calculated with the following equation given by Dulk (1985) in the optical thin regime,

$$T_{\rm B} = 9.78 \times 10^{-3} \frac{\rm EM}{\nu^2\, T^{1/2}} \times (24.5 + \ln(T/\nu)) \qquad (1)$$

where $T_{\rm B}$ (K) is the brightness temperature, EM $= n^2 L$ is the total emission measure (n (cm^{-3}) is the number density and L (cm) is the column depth), T (K) is the plasma temperature, and ν (Hz) is the frequency. For the event of study, two groups of authors have done the DEM analysis using different methods (Liu et al. 2013; Sun et al. 2014). Here, we simply read the published numbers of the DEM-weighted average T and EM, without repeating the DEM analysis. Comparing Figure 6 of Liu et al. (2013) and Figure 11 of Sun et al. (2014), we see that results of the two studies are qualitatively similar, with the flux rope outlined by regions of high T and EM, yet both parameters are still significantly less than those in the flare loops. Within the C1 region defined in Figure 3(d), around 04:50 UT we read from Sun et al. (2014) that T is in a range of ~6–8 MK and EM is in a range of ~1–2.5 $\times 10^{28}$ cm^{-5}, and from Liu et al. (2013) that T varies from 3–6 MK and EM varies from 1–2 $\times 10^{28}$ cm^{-5}. With these numbers, we obtain that the thermal $T_{\rm B}$ at 17 GHz varies in a range of 2000–6000 K. Assuming that there is not sufficient material cooler than these temperature ranges to contribute significantly to the brightness temperature, the NoRH brightness temperatures appear to require a non-thermal contribution.

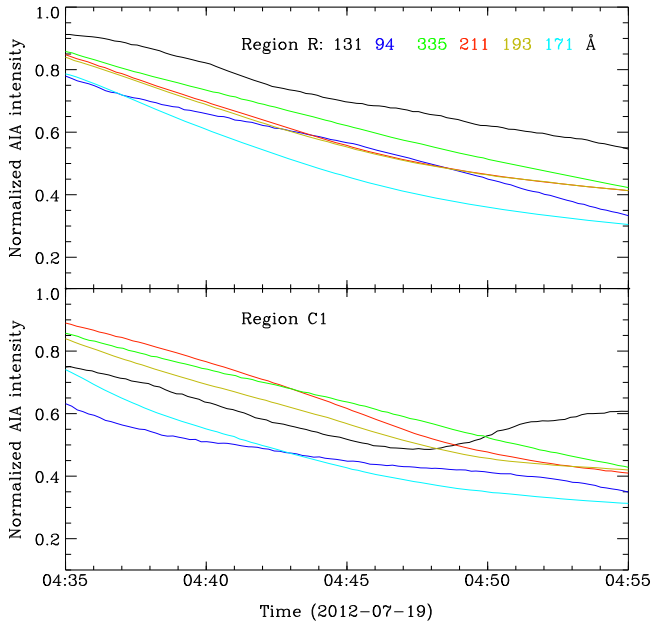

Figure 5. AIA light curves at 131, 94, 335, 211, 193, and 171 Å from 04:35 to 04:55 UT. The data are normalized to corresponding values at 04:30 UT.

To further show that at least the oscillating part of the microwave signals is non-thermal, we examine temporal variations of light curves of different AIA passbands that are related to thermal plasmas to see whether a similar 2 minute oscillation exists or not. If not, we may attribute that the microwave oscillation reported above belongs to non-thermal emission of energetic electrons. To do this, we plot in Figure 5 the light curves observed with the AIA 131, 94, 335, 211, 193, and 171 Å passbands from 04:35 to 04:55 UT in the flux rope region (upper panel) and C1 region (lower panel). We see that in these EUV channels, the light curves vary rather smoothly with most curves declining gradually (due to the rise and expansion of the flux rope) without any notable oscillations. This further supports that at least the oscillating component of the microwave sources is given by non-thermal energetic electrons, possibly through the gryo-synchrotron emission mechanism (Dulk 1985).

5. CONCLUSIONS AND DISCUSSION

Investigating pre-impulsive processes is of crucial importance to understanding the physics leading to explosive energy release of solar eruption. Here, we present such a study using microwave imaging data of a flux rope structure observed during the pre-impulsive phase of the M7.7 flare on 2012 July 19. Previous studies on the same event already showed the flux rope is of high temperature and is connected to the flare reconnection region. Based on these studies, we focus on the microwave data at 17 GHz obtained by NoRH to reveal the microwave characteristics of the same structure. We find that the flux rope, while being hot in general, contains microwave-emitting energetic electrons. The flux rope, as viewed in the microwave, exhibits several local maxima of emission intensities with relatively fixed locations. These maxima,

i.e., microwave islands, are bridged by generally weaker emission, forming an overall arcade-like structure.

We also show that the flux rope microwave sources seem at least partly due to non-thermal energetic electrons, possibly at energies of hundreds of keV (e.g., Kundu et al. 2001, 2004; White et al. 2011). High localization of these microwave sources indicates that the energetic electrons may be affected or confined by the large-scale magnetic structure within the flux rope. The confinement is probably via the well-known magnetic mirror effect if local magnetic enhancements are present. These magnetic enhancements can be due to twisting flux rope field lines and/or their interaction with nearby magnetic structures. Thus, the microwave islands can be used to infer sites of magnetic enhancements within the flux rope structure, which are at present very difficult, if not impossible, to measure directly.

It is also found that the microwave emission is characterized by a 2 minute oscillation period. The period agrees well with the occurrence rate of the AIA-observed contracting loops and ejective plasmoids that are manifestations of reconnection outflows during the pre-impulsive stage. This correlation indicates that the microwave periodicity is associated with the reconnection that takes place and releases energetic electrons intermittently every ~2 minute interval. Note that oscillations with similar periodicity during flares have been reported and attributed to flare-released fast magnetosonic wave trains (e.g., Ofman et al. 2011; Liu et al. 2012; Yang et al. 2015), or some external modulations by disturbances associated with the sunspot (Sych et al. 2009; Reznikova & Shibasaki 2011) or the photosphere/chromosphere oscillations (Kislyakova et al. 2011). These independent observational findings, together with ours, point to an intermittent nature of the flaring reconnections, not only during their impulsive stage but also in the pre-impulsive stage.

This work was partly carried out on the Solar Data Analysis System operated by the Astronomy Data Center in cooperation with the Solar Observatory of the National Astronomical Observatory of Japan. We are grateful to the *SDO* teams for making their data available to us. Z.W. thanks Qiang Hu and Xing Li for useful discussions. This work was supported by grants NSBRSF 2012CB825601, NNSFC 41274175, and 41331068. G.L.'s work at UAHuntsivlle was supported by NSF grants ATM-0847719 and AGS1135432.

REFERENCES

Aschwanden, M. J., Boerner, P., Schrijver, C. J., et al. 2013, SoPh, 283, 5
Chen, J. 1996, JGR, 101, 27499
Cheng, X., Zhang, J., & Ding, M. D. 2013, ApJ, 763, 43
Dulk, G. A. 1985, ARA&A, 23, 169
Forbes, T. G. 2000, JGR, 105, 23153
Kislyakova, K. S., Zaitsev, V. V., Urpo, S., et al. 2011, ARep, 55, 275
Krucker, S., & Battaglia, M. 2014, ApJ, 780, 107
Kundu, M. R., Garaimov, V. I., White, S. M., et al. 2004, ApJ, 600, 1052
Kundu, M. R., Nindos, A., & White, S. M. 2001, ApJ, 557, 880
Lemen, J. R., Title, A. M., Akin, D. J., et al. 2012, SoPh, 275, 17
Lin, R. P., Dennis, B. R., Hurford, G. J., et al. 2002, SoPh, 210, 3
Liu, R. 2013, MNRAS, 434, 1309
Liu, W., Chen, Q., & Petrosian, V. 2013, ApJ, 767, 168
Liu, W., Ofman, L., Nitta, N. V., et al. 2012, ApJ, 753, 52
Low, B. C. 2001, JGR, 106, 25141
Low, B. C., & Hundhausen, J. R. 1995, ApJ, 443, 818
Masuda, S., Kosugi, T., Hara, H., et al. 1994, Natur, 371, 495
Morgachev, A. S., Kuznetsov, S. A., & Melnikov, V. F. 2014, Ge&Ae, 54, 933
Nakajima, H., Nishio, M., Enome, S., et al. 1994, IEEEP, 82, 705
Narukage, N., Shimojo, M., & Sakao, T. 2014, ApJ, 787, 125
Ofman, L., Liu, W., Title, A., et al. 2011, ApJL, 740, L33
Patsourakos, S., Vourlidas, A., & Stenborg, G. 2013, ApJ, 764, 125
Pesnell, W. D., Thompson, B. J., Chamberlin, P. C., et al. 2012, SoPh, 275, 3
Reznikova, V. E., & Shibasaki, K. 2011, A&A, 525, 112
Song, H. Q., Chen, Y., Zhang, J., et al. 2015, ApJL, 808, L15
Song, H. Q., Zhang, J., Chen, Y., et al. 2014, ApJL, 792, L40
Sun, J. Q., Cheng, X., & Ding, M. D. 2014, ApJ, 786, 73
Sych, R., Nakariakov, V. M., Karlicky, M., et al. 2009, A&A, 505, 791
Takano, T., Nakajima, H., Enome, S., et al. 1997, LNP, 483, 183
White, S. M., Benz, A. Q., Christe, S., et al. 2011, SSRv, 159, 225
Yang, L., Zhang, L., He, J., et al. 2015, ApJ, 800, 111
Zhang, J., Cheng, X., & Ding, M. D. 2012, NatCo, 3, 747